Received: 13 May 2019 | Revised: 23 November 2019 | Accepted: 23 November 2019

DOI: 10.1002/eng2.12082

RESEARCH ARTICLE

WILEY

Design, modeling, and experimental validation of a concave-shape pectoral fin of labriform-mode swimming robot

Farah A. Naser | **Mofeed T. Rashid**

Electrical Engineering Department, University of Basrah, Basrah, Iraq

Correspondence
Mofeed T. Rashid, Electrical Engineering Department, University of Basrah, Basrah, Iraq.
Email: mofid76@gmail.com

The pectoral fin shape, size, and speed are the three main parameters for the proposed design. The influence of the geometrical shape of pectoral fin in labriform-mode swimming mechanism is evaluated with the aid of computational fluid dynamics (CFD) method, which could be considered as a first step before building the complete robot prototype. The simulated results obtained are then validated experimentally. Two concave-shape fins were designed with high precision, and each one of them is attached to a servomotor arm, which is, in turn, connected to a servomotor that is sliding on a pair of parallel shafts fixed at the center of a pool. The mathematical model of the proposed design is derived and then simulated by SolidWorks software. A different number of fin oscillating angles are tested with different power-to-recovery ratios. The generated thrust and drag force components under different working conditions are investigated, and hence, the drag coefficient is obtained experimentally. Body velocity and motor torque are calculated and compared with theoretical analysis. The results indicate that for each angle of rotation, there exists an optimal ratio that produces a maximum thrust during power stroke and maintains a minimum drag during recovery stroke.

KEYWORDS

computational fluid dynamics, labriform mode, pectoral fin, power-to-recovery ratios, swimming robot

1 | INTRODUCTION

A large number of applications require the use of swimming robots such as aquatic life monitoring, military intervention, water pollution detection, and commercial applications. These all involve the continuous development of underwater robots, which can be used instead of human beings.[1] Designing the swimming robots to behave like real fish in terms of movement and maneuvering requires a deep knowledge of swimming mode mechanisms and behaviors. Different types of fish use different types of fins as their main locomotor. Generally, there are two types of swimming modes: body and/or caudal fin (BCF) and median and/or pectoral fin (MPF), and according to the type of fins that

uses in locomotion, they can be further classified into undulatory type and oscillatory type.[2] For BCF-undulatory type, the motion is a wave of muscles that is generated from the head of the fish to its tail such as anguilliform, carangiform, and subcarangiform locomotion, whereas the oscillation motion involves turning of the body and caudal fin to propel the fish such as ostraciiform and thunniform locomotion. On the other hand, the MPF undulatory motion involves diodontiform, gymnotiform, amiform, and balistiform locomotion and oscillatory motion such as labriform and tetadntiform. Another type known as rajiform can be considered as a combination of undulatory and oscillatory locomotion.[3]

In the literature, there are many studies about swimming robots' design and modeling that uses the pectoral fins as the main locomotor; researchers in References 4-6 developed a fish-like swimming robot based on artemia and provided a wireless control mechanism that controls the movement of underwater robot. Reference 7 provided a robotic fish with oscillating pectoral fins, and the way it is controlled was done by central pattern generators (CPGs). Others in Reference 8 developed a cownose ray-inspired robotic fish where the propulsion mechanism was by both oscillating and chordwise twisting pectoral fins. In Reference 9, the researchers designed and studied the effect of pectoral fin flexibility in the performance of robotic fish. We utilize this fact in our proposed model since fin rigidity is a crucial issue in producing high thrust. An integrated approach of both insect wings and fish fins was proposed in Reference 10 for higher agility achievement underwater. In Reference 11, researchers considered the turning characteristics of robotic fish with 2-degree of freedom pectoral fins and flexible body/caudal fin. They examined the hydrodynamic forces with three cases of propulsion mechanisms: both sides of pectoral fins, flexible body/caudal fin, and composite of them. A new hybrid tail fish robot, which is actuated by two active joints, is developed. The first joint is responsible for forward motion and driven by a servomotor, whereas the second joint is actuated by a soft actuator, an ionic polymer-metal composite (IPMC) artificial muscle, which directs the propelled fluid for steering.[12]

The researchers in Reference 13 proposed an evolutionary multiobjective optimization (EMO) approach to the design and control of flexible fins for robotic fish, in which they investigated fins of different stiffness values and sizes. In Reference 14, the authors mentioned the unmanned underwater vehicles (UUVs) by studying the hydrodynamics of UUVs, especially drag force since it is required to determine the total thrust. Reference 15 provided a perfect design of autonomous underwater vehicle of marine propeller with the aid of both computational fluid dynamics (CFD) simulation and finite element analysis method by SolidWorks software in order to get the optimum thrust from the propeller. In Reference 16, the authors developed a dynamic model of the oscillating pectoral fin based on the quasi-steady blade element theory, and they investigated different motion parameters to show the performance of the oscillating pectoral fin. A 6-DOF of robotic fish is adopted in Reference 17, in which surge, sway, heave, roll, pitch, and yaw were considered as the swimming in ocean with the carangiform-mode swimming mechanism.

In labriform (rowing motion)-mode swimming mechanism, the main component of the hydrodynamics force is due to the drag force.[18-22] Pectoral fins are the major elements in the fish, which produce forward thrust force.[23] In Reference 24, the researchers presented both the sensory feedback attitude control of a bio-inspired robotic fish with pectoral fin actuation. Single undulating fin propulsion mechanism, for the swimming robot, was developed and tested in Reference 25, and the fin controls both forward motion and directional maneuvers. A complete three-dimensional (3D) dynamic model for the robotic fish actuated by pectoral and caudal fins is presented in Reference 26, in which the fluid forces mainly contain quasi-steady lift and drag, gravity and buoyancy, and waterjet strike force. In Reference 27, a study of the relationship between pectoral-fin ray stiffness and swimming behavior in Labridae is given in detail in terms of design, performance, and ecology.

In this article, the design and modeling of pectoral fins of labriform-mode swimming robot are implemented. The main contribution of this article is to present a dynamic model of a concave fin that produces hydrodynamic forces for swimming robot based on pectoral fin as a rigid body, which, in turn, plays a significant role in picking up the body rotation and transition motions of a swimming robot. The concave shape provides a reaction force that will support and help in the propulsion mechanism during the power stroke, while during recovery stroke, it will be at minimum. This model is concerned with the variation of the rotation angle between the longitudinal axis of the pectoral fin and the main direction of the water flow, which, in our case, is defined as (Θ). The proposed model analysis is enhanced using CFD method and practical experiments, and both simulated and experimental results showed the effectiveness of such a model in producing forward thrust force.

The remainder of this article is organized as follows. Pectoral fins of the robotic fish prototype are briefly introduced in Section 2. Section 3 presents the mathematical model of the proposed design. Analyses of simulation/experimental results are further offered in Section 4. Section 5 includes the conclusion.

2 | DESIGN OF PECTORAL FINS

During the movement of fluid through an object, there should be a resistance to that movement. This resistance generates a hydrodynamic force, which can be classified into force due to the friction and force due to the pressure. These two forces may incorporate together with the geometrical shape, speed, and characteristics of the fluid in producing forward velocity. Navier-Stokes equations are solved by computational fluid dynamics that is an incredible powerful tool provided by SolidWorks software, which can be utilized in identifying these hydrodynamic forces.[28] In our proposed model, two servomotors, two pectoral fins, and two joints were carefully designed by SolidWorks software, as shown in Figure 1.

Physically and geometrically, the movement of the body in a fluid may result in displacement of a portion of the fluid within the movement of the body and results in moving that displaced fluid with the body, producing an effect of added mass.[15,29] Servomotor joint was designed very precisely to match the servo's shaft. Two joints were attached to each servomotor to satisfy the motion dictated by the servomotor such that the pectoral fin maintains the highest speed during the power stroke and the lowest speed during the recovery stroke. The two servomotors were linked with pectoral fins through their arms and then placed on a thin plate, as shown in Figure 2, which in turn slides over two parallel shafts (in order to investigate the drag force generated from the pectoral fins only) placed in a pool with a specific dimension. The complete prototype design of the pectoral fins experiment is shown in Figure 3. This robot is assumed to be surrounded

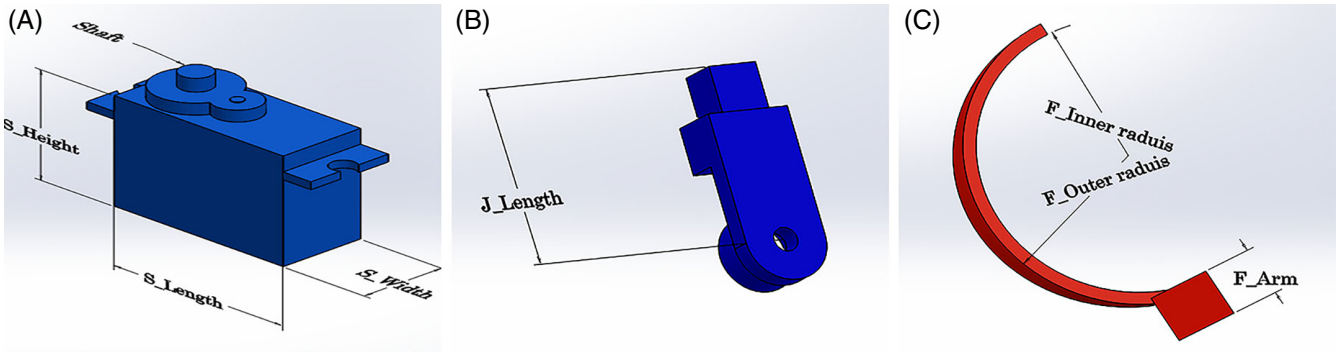

FIGURE 1 The components of the proposed design. A, Servomotor. B, Servomotor arm. C, Concave pectoral fin

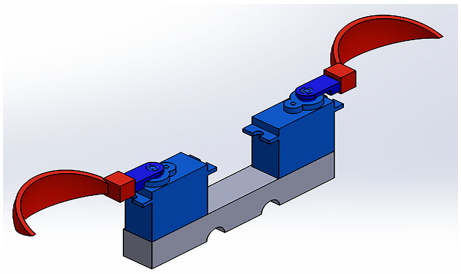

FIGURE 2 Left and right pectoral fins attached to their servomotors

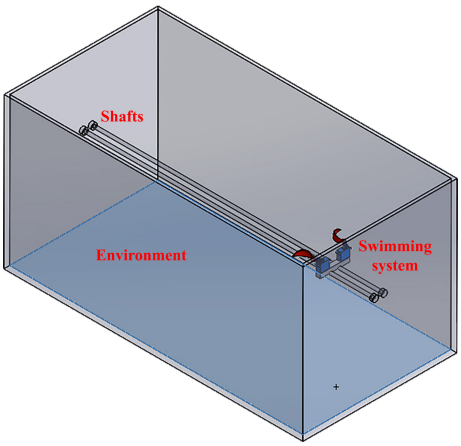

FIGURE 3 The complete design of experiment

by an inviscid, incompressible fluid.[28-30] In Reference 29, the depth of the robot is kept unchanged during swimming, ignoring the effect of the pressure in this simulation.

3 | MATHEMATICAL MODEL OF THE PROPOSED DESIGN

We assumed that the body's frame coincides with the global coordinate system. Since we are concerned with only the pectoral fins at this stage, the movement of the body is a 1-DOF, which is represented by the linear velocity component along the x-axis. A top view of free body diagram is shown in Figure 4, where $[X, Y, Z]^{\mathrm{T}}$ indicates the global robotic fish. We followed the simplified equations of the fish body in the body coordinate system, as represented in References 9, 16, and 28.

$$(M_b - M_{ax})\dot{V}_{bx} = (M_b - M_{ax})V_{bz}w_{by} + F_x, \tag{1}$$

$$(I_y - M_{ay})\dot{w}_{by} = M_y, \tag{2}$$

$$(M_b - M_{az})\dot{V}_{bz} = (M_b - M_{ax})V_{bx}w_{by} + F_z, \tag{3}$$

where M_b is the robotic fish mass, I_y is the robot inertia about the y-axis, and M_{ax}, M_{ay}, and M_{az} are the added mass/inertia on the rigid body.[9,16,31,32] V_{bx}, w_{by}, and V_{bz} are the body's x, y, and z velocity components, respectively. F_x, M_y, and F_z are the external hydrodynamics forces/moments exerted on the robotic fish body, which are given as

$$F_x = F_{hx} - F_{\mathrm{D}}\cos\beta + F_{\mathrm{L}}\sin\beta, \tag{4}$$

$$M_y = M_{hy} + M_{\mathrm{D}}, \tag{5}$$

$$F_z = F_{hz} - F_{\mathrm{D}}\sin\beta - F_{\mathrm{L}}\cos\beta, \tag{6}$$

where F_{hx}, M_y, and F_z are the hydrodynamic forces/moments transmitted from the pectoral fins to the robotic fish. F_{D}, M_{D}, and F_{L} are the body's drag, moment, and lift forces, respectively. These forces are given as follows:

$$F_{\mathrm{D}} = \frac{1}{2}\rho V_b^2 S C_{\mathrm{D}}, \tag{7}$$

$$M_{\mathrm{D}} = -C_{M w_{by}}\mathrm{sgn}(w_{by}), \tag{8}$$

$$F_L = \frac{1}{2}\rho V_b^2 S C_L \beta, \tag{9}$$

$$V_b = \sqrt{V_{bx}^2 + V_{bz}^2}. \tag{10}$$

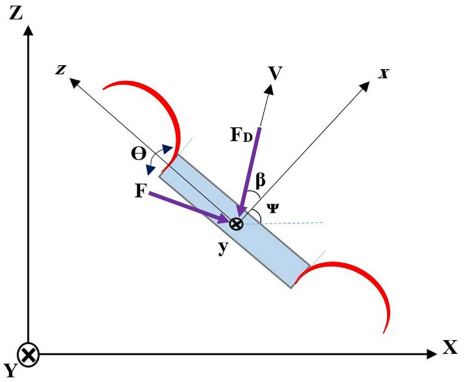

FIGURE 4 The free body diagram of the pectoral fins

The robot kinematics are given as in References 13 and 15

$$\dot{X} = V_{bx}\cos\Psi - V_{bz}\sin\Psi, \tag{11}$$

$$\dot{Y} = w_{by}, \tag{12}$$

$$\dot{\Psi} = V_{bz}\cos\Psi + V_{bx}\sin\Psi, \tag{13}$$

where ρ is the water density and Ψ is the angle between the x-axis of global coordinate and the x-axis of body coordinate. C_{D} and C_{L} are the drag and lift coefficients, respectively, while S denotes the projected surface area to the water such that

$$S_{\mathrm{outer}} = [4\pi(r_{\mathrm{outer}})^2]/8, \tag{14}$$

$$S_{\mathrm{inner}} = [4\pi(r_{\mathrm{inner}})^2]/8, \tag{15}$$

where S_{outer} and S_{inner} are the surface areas of outer and inner radii, respectively, while r_{outer} and r_{inner} are the fin outer radius and fin inner radius, respectively. β is defined as the angle of attack of the body, and sgn(.) is the signum function, and Ψ is the angle between the x-axis and the X-axis.[28]

Generally, the drag force is the force that is in the opposite direction to the flow and the lift force is the normal force to the flow.[21] In order to evaluate the hydrodynamic force applied by the water, we set up the proposed model as stationary and let the water be the moving part. The servomotor is employed to a rotating fin based on the following equation, with the rotation pattern shown in Figure 5.

$$\theta(t) = \frac{A}{2} - \frac{A}{2}\cdot\cos\omega t, \tag{16}$$

where $\Theta(t)$ represents the instantaneous angular position of the base of the fin, A is the amplitude of the wave generated by the fin, and ω is the angular frequency that can be given as $\omega = 2\pi f$.[20,33,34] Only the forward direction of swimming is considered. Our main goal is to determine the hydrodynamic forces applied to the pectoral fin while moving toward or backward within different fin beat angles.

In order to get net thrust, we followed this fact:

$$\mathrm{Net}_{\mathrm{Thrust}} = \sum_{\theta^\circ}^{-\theta^\circ} \mathrm{Thrust} - \sum_{-\theta^\circ}^{\theta^\circ} \mathrm{Drag}, \tag{17}$$

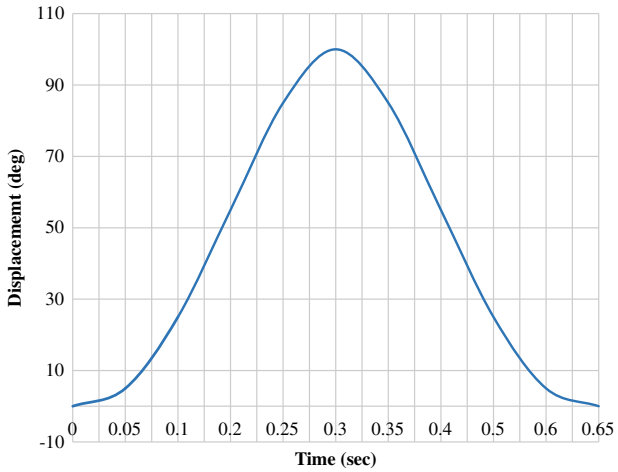

FIGURE 5 Servomotor rotation angle

where the hydrodynamic forces at each angle of rotation are calculated and added to the previous angle until completing on cycle. It is noteworthy that we use the sign (−) before the angle to indicate the recovery stroke side, whereas the positive angle is the starting angle at the power stroke.

4 | EXPERIMENTS AND RESULTS

4.1 | Simulation analysis

To validate the proposed design, five experiments of different power-to-recovery ratios are conducted on the robot model, in which a pair of pectoral fins is designed with plastic polylactic acid (PLA) as a rigid material with a density of 1300 kg/m^3. The novel design of these fins is precisely built as an octal hollow spherical shape such that the outer radius is 2.5 cm and the inner radius is 2.3 cm, producing a rigid concave shape of thickness 2 mm. A joint of length 1.88 cm is driven by a servomotor, which is connected to a well-designed joint attached to each pectoral fin. Since our model is based on rowing motion of the labriform mode, during power stroke phase, the thrust force should be at a maximum value, whereas in recovery stroke phase, it is strongly recommended to minimize the drag force as much as possible in order to generate a net forward thrust. We utilize the concave shape of the pectoral fin to produce the maximum thrust during the power stroke and the minimum drag force during recovery stroke, where the net forward thrust = thrust − drag. We tested our model with different power-to-recovery stroke ratios (ie, a ratio of 1:1, 2:1, 3:1, 4:1, and 5:1), and in each ratio, we further tested the model with different oscillating ranges. Due to our model geometry of a concave fin design, we use the maximum angle 50° in power, so the fin will not hit the frontal part of the body.

The following assumptions were used for both power stroke and recovery stroke:

- Air pressure is 101 325 pa at 20°C (293 K).
- Gravity feature is considered, where $g = 9.81$ m/s^2.
- The dimensions of the proposed tank (computational domain) are set as 1 m × 0.65 m × 0.65 m.
- We assumed the roughness is 0 μm.
- No cavitation is in the simulation.
- Water density is 1000 kg/m^3.
- Projected surface area is 0.0813 m^2 in power stroke and 0.0947 m^2 in recovery stroke.
- Plate of the servos' dimensions is 0.1 × 0.12 × 0.01 m.
- Servomotor speed is 0.11 second/60°.
- Oscillating frequency is 1.515 Hz.
- The servomotor arm is at 50° at reset.
- Boundary condition is set to ideal wall (ie, no slip condition).
- *XYZ* earth global coordinate coincides with the *xyz* body coordinate systems.
- Mass of each fin is 8.82 g.
- For this prototype, we ignored added mass/inertia effect.
- The total hydrodynamic forces exerted on the pectoral fins are in the x direction, while the hydrodynamic force in y and z directions are both zero because of the left-right symmetry of the oscillating fins. Consequently, we are concerned with the forward velocity of the body at the *x*-axis, and other velocity components on *y*- and *z*-axes are zeros.

With the aid of CFD, we investigate the thrust and drag for every angle of rotation starting from 50°, 40°, 30°, 20°, 10°, 0°, −10°, −20°, −30°, −40°, and −50°. Each angle is tested for both power stroke speed and recovery stroke.

For each case in Figure 6, there is an optimal range of oscillation with optimal power-to-recovery ratio; for the ratio of 1:1, the optimal range is 10° to −10°, which is translated to an amplitude of 20° and so on for other ranges. The moderate ratio 3:1 can be considered as an optimal range with approximately all different ranges. As the range increases, the hydrodynamic force will be accumulated following Equation (17); we validate this fact as shown in Figures 7-11.

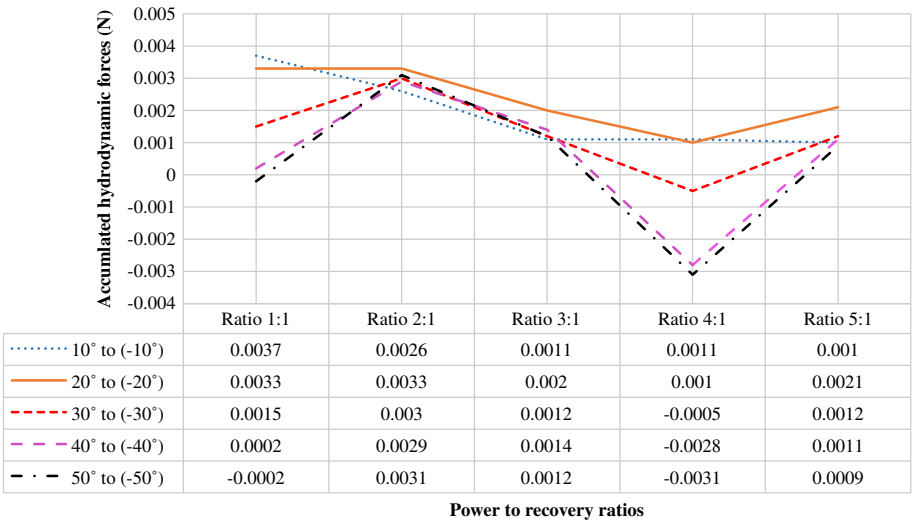

	Ratio 1:1	Ratio 2:1	Ratio 3:1	Ratio 4:1	Ratio 5:1
10° to (-10°)	0.0037	0.0026	0.0011	0.0011	0.001
20° to (-20°)	0.0033	0.0033	0.002	0.001	0.0021
30° to (-30°)	0.0015	0.003	0.0012	-0.0005	0.0012
40° to (-40°)	0.0002	0.0029	0.0014	-0.0028	0.0011
50° to (-50°)	-0.0002	0.0031	0.0012	-0.0031	0.0009

FIGURE 6 Hydrodynamic forces vs different ranges of power-to-recovery stroke ratios

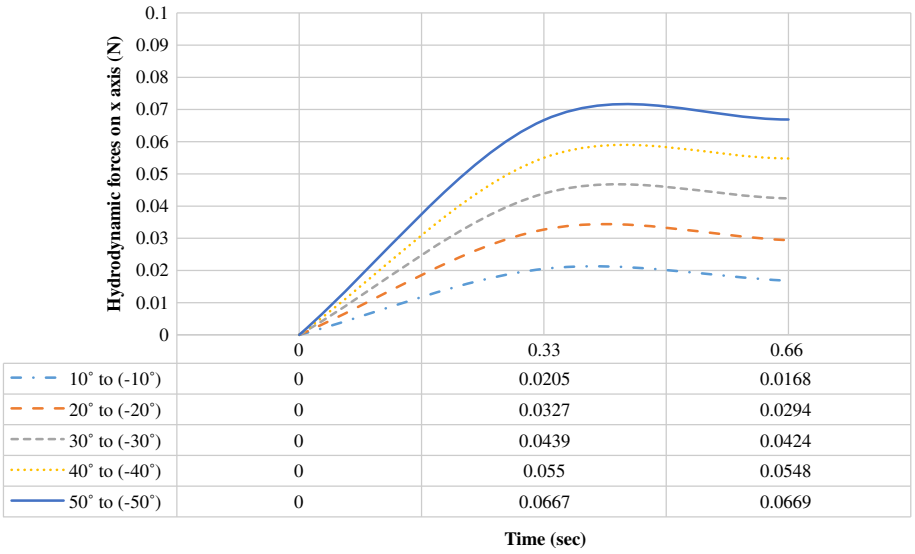

	0	0.33	0.66
10° to (-10°)	0	0.0205	0.0168
20° to (-20°)	0	0.0327	0.0294
30° to (-30°)	0	0.0439	0.0424
40° to (-40°)	0	0.055	0.0548
50° to (-50°)	0	0.0667	0.0669

FIGURE 7 Hydrodynamic forces on *x*-axis (N) when power-to-stroke ratio is 1:1

The results showed that the maximum thrust can be achieved at 50° and the minimum drag is at −50°, producing a total angular displacement of 100° around the *y*-axis. The hydrodynamic forces are applied to both concave and convex sides when the fin starts to beat in power stroke cycle, for a power-to-stroke ratio of 1:1, the active force is the forward thrust force and is applied from 0 to 0.33 seconds, while in recovery stroke, the active force is the drag force, which is in the opposite direction of robot's forward movement and is applied from 0.33 to 0.66 seconds to complete one cycle, as shown in Figure 12, where the red arrows indicate the motor motion and the blue ones represent the applied hydrodynamic forces. For other ratios, the same manner is followed, where each time corresponds to a specific power-to-recovery ratio.

The drag coefficient is calculated, and for comparison purposes, we compared the calculated drag coefficient with the one in the literature; the results showed approximately the same as mentioned in References 9, 28, and 35, as shown Figure 13 at power-to-recovery ratios of 1:1 and 2:1 at different angles of rotation.

For theoretical verifications, we will consider the ratio of 1:1 with an oscillating range of 50° to −50°. Following Equation (16), the angular velocity of the fin at power stroke speed at time 0.33 second is about 303°/second; this value matches the theoretical calculations by the relation $\omega = \Theta/t$, where Θ is 100° (1.74 rad/second) and t is 0.33 second, which gives the angular velocity of 5.27 rad/second (301.99°). Figure 14 shows the simulation result of angular fin velocity.

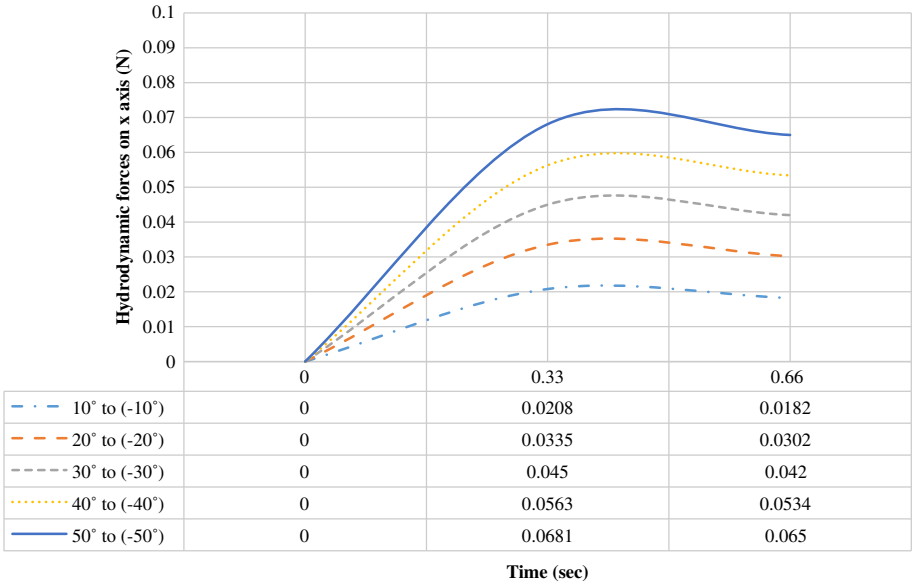

	0	0.33	0.66
10° to (-10°)	0	0.0208	0.0182
20° to (-20°)	0	0.0335	0.0302
30° to (-30°)	0	0.045	0.042
40° to (-40°)	0	0.0563	0.0534
50° to (-50°)	0	0.0681	0.065

FIGURE 8 Hydrodynamic forces on *x*-axis (N) when power-to-stroke ratio is 2:1

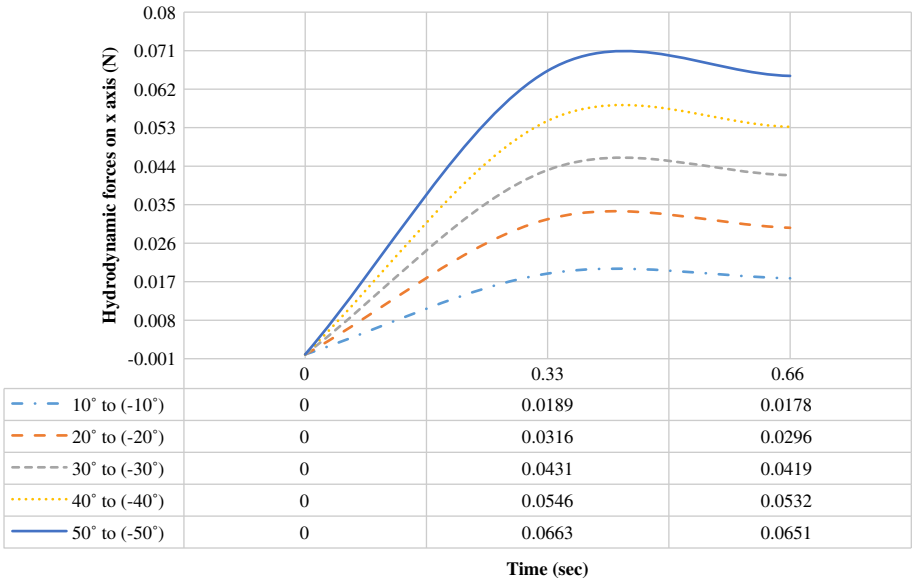

	0	0.33	0.66
10° to (-10°)	0	0.0189	0.0178
20° to (-20°)	0	0.0316	0.0296
30° to (-30°)	0	0.0431	0.0419
40° to (-40°)	0	0.0546	0.0532
50° to (-50°)	0	0.0663	0.0651

FIGURE 9 Hydrodynamic forces on *x*-axis (N) when power-to-stroke ratio is 3:1

The corresponding body velocity is then calculated with and without the hydrodynamic force in Figure 15. The body velocity reaches about 5 to 10 cm/second. It is good to remention that we ignored both friction and weight of the plate and consider only the effect on the pectoral fin to examine its ability to produce the net thrust. The simulated results given here prove its success. For the same case, we calculated the motor torque required to oscillate the pectoral fin with and without the hydrodynamic force and is shown in Figure 16, where the results match the theoretical calculation with motor torque = applied force × radius; since the applied force is considered only on the fins without taking into account the other components, the motor torque is very small at this stage. The magnitude of angular velocity is calculated for complete cycle of the fin, which matches the theoretical results, where the power stroke speed is 5.27 rad/second as calculated previously and the recovery stroke speed is also 5.27 rad/second (1.74 rad/0.66 second) and the total angular velocity for both power and recovery strokes is (300° + 300°)/second, as shown in Figure 17. From the previous results, we calculated the forward linear velocity of the body during one cycle when the power-to-recovery ratio is 1:1, 2:1, 3:1, 4:1, and 5:1, as shown in Figure 18.

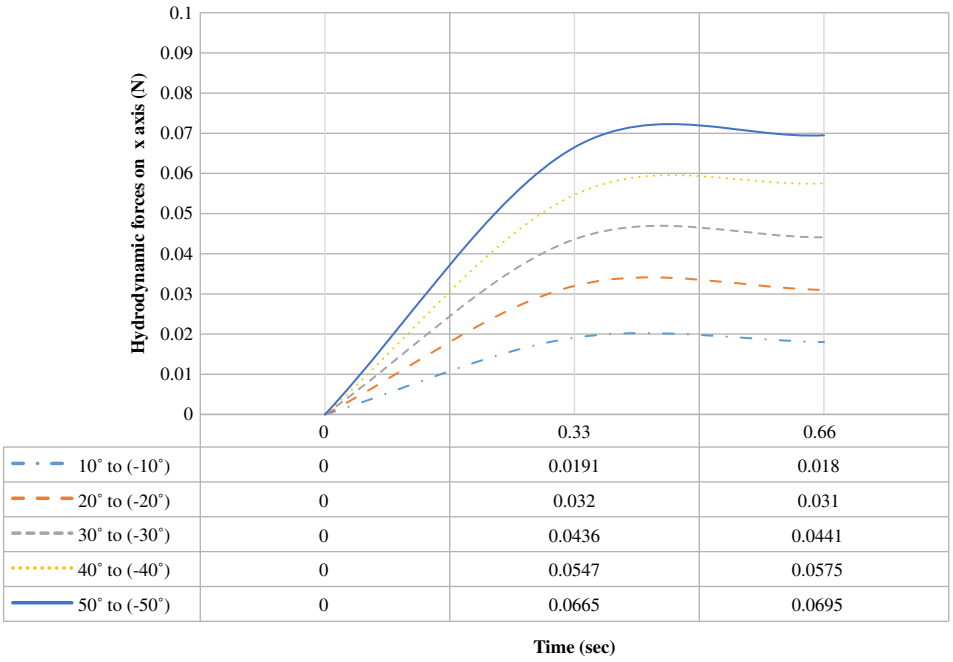

FIGURE 10 Hydrodynamic forces on *x*-axis (N) when power-to-stroke ratio is 4:1

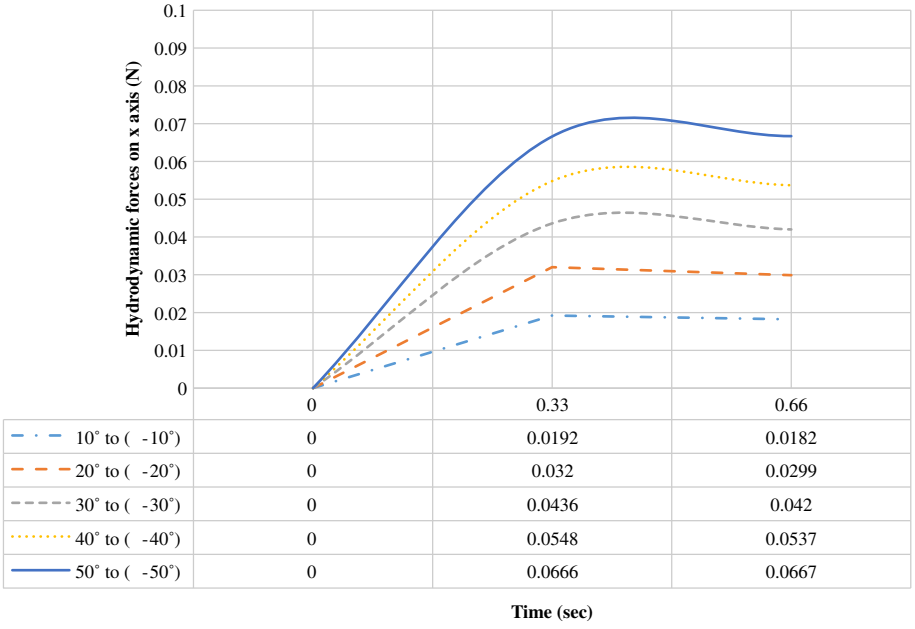

FIGURE 11 Hydrodynamic forces on *x*-axis (N) when power-to-stroke ratio is 5:1

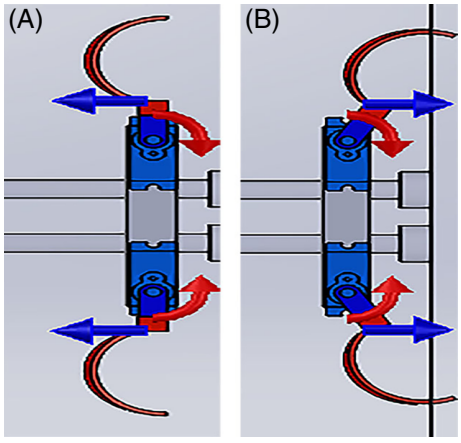

FIGURE 12 Thrust and drag forces at power and recovery strokes. A, Power stroke. B, Recovery stroke

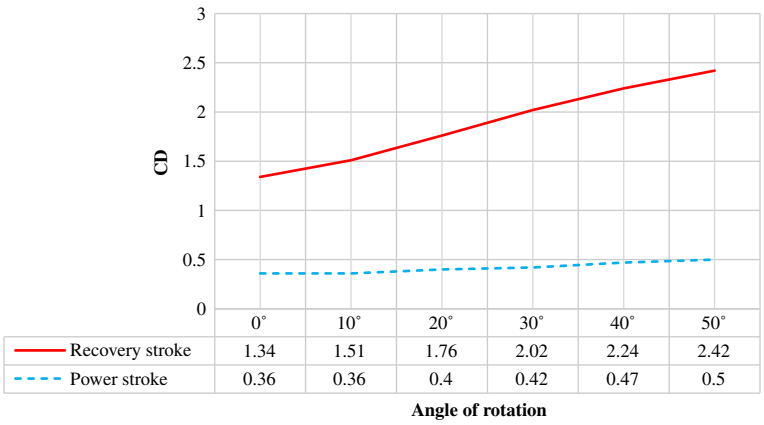

FIGURE 13 Drag coefficient at power and recovery strokes

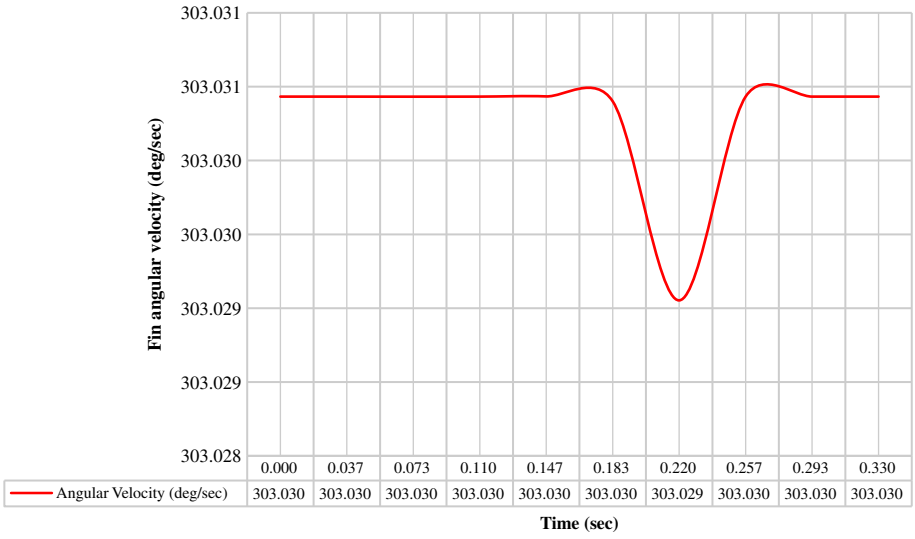

FIGURE 14 Angular velocity of the pectoral fin at power-to-stroke ratio of 1:1

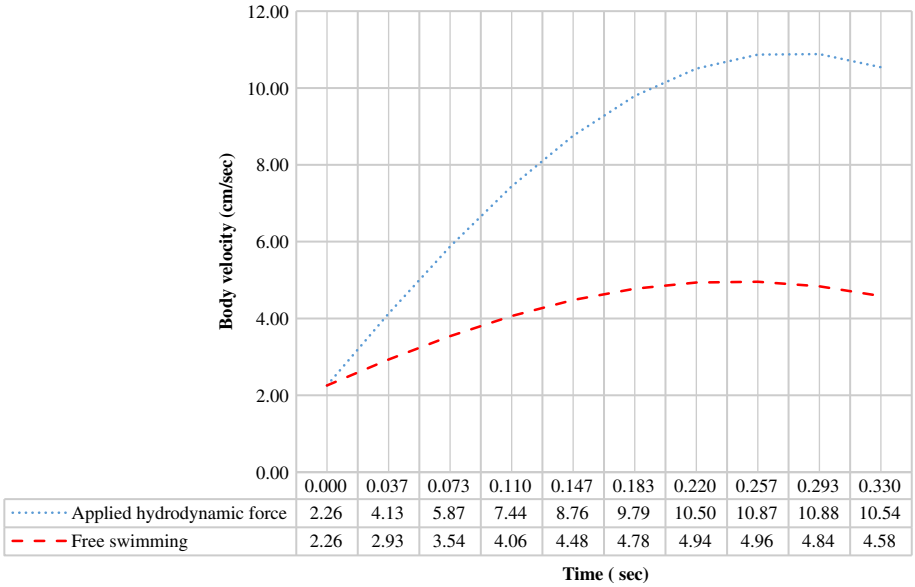

FIGURE 15 Body forward velocity at power stroke time

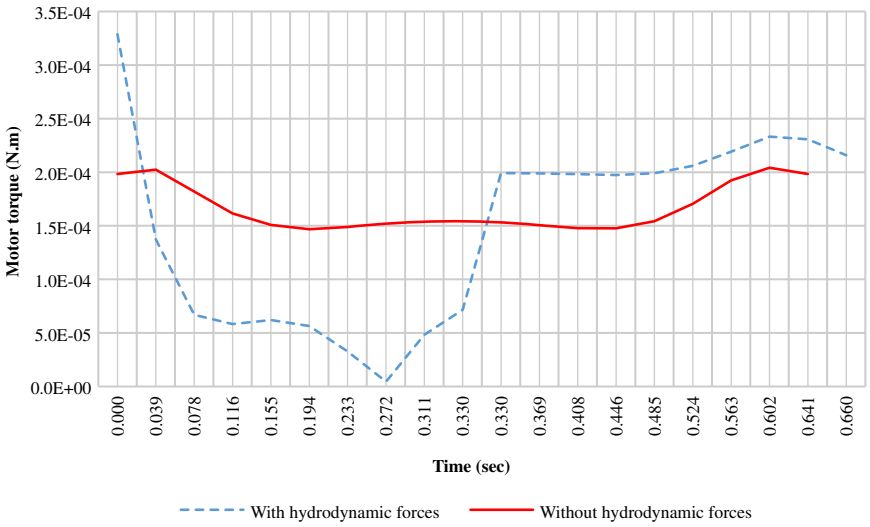

FIGURE 16 Motor torque at power and recovery stroke times

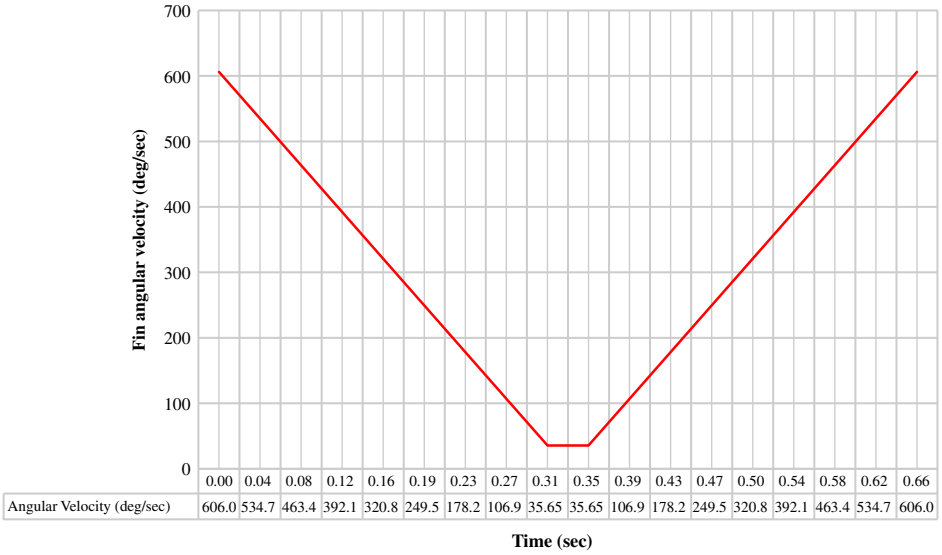

FIGURE 17 Angular velocity of the fin during one cycle

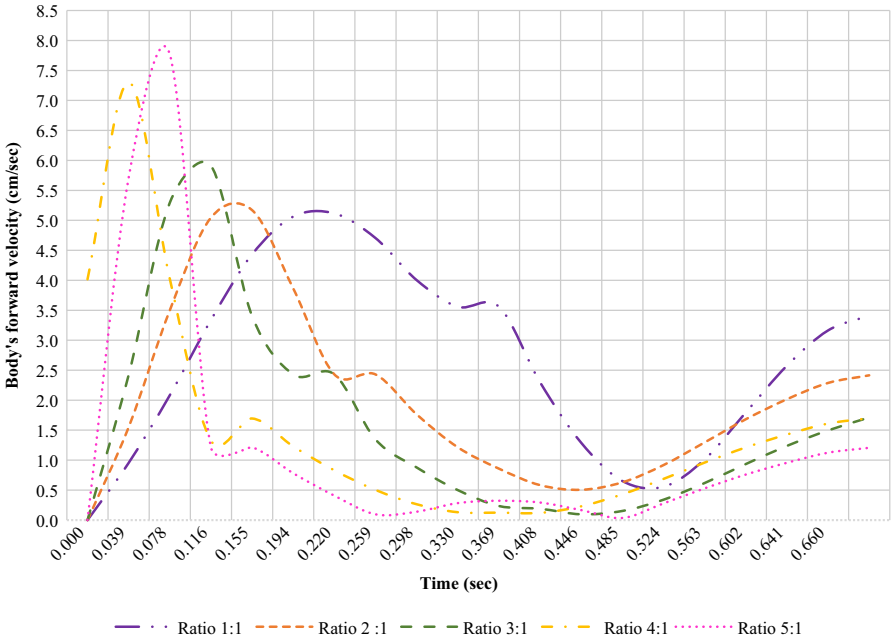

FIGURE 18 Forward body velocity with different power-to-recovery ratios

4.2 | Experimental analysis

In this section, experimental results validating the accuracy of the model developed in the previous section are given. A swimming pool of dimension of 1 m × 0.65 m × 0.65 m made of acrylic plastic material has been used as an experiment environment, and the pectoral fins of the robot are controlled by an Atmega microcontroller, while Waterproof Sub-Micro Servo from Traxxas was used to move the pectoral fins at the maximum speed of 0.11 second/60°. All plastic parts such as fins, joints, and base plates are made by a 3D printer of PLA material. The robot motion was captured through Kodak high-resolution camera at a frame rate of 30 frames per second. A computer equipped with MATLAB software, capable of supporting real-time and offline workflows, was used to extract the desired data and process the video via image processing toolbox. Two stainless steel parallel shafts used as motion straighter are fixed in the middle of the tank at a height of 32.5 cm; about half of the pool is filled with water to make the robot neutrally buoyant. The robot is driven by wires, which are connected to the 5-V power supply. Figures 19-21 show the complete setup process of the experiment.

Five power-to-recovery stroke speed ratios were tested. In all simulations/experiments, the maximum servomotor speed is fixed, which corresponds to a fin-beat frequency of 1.515 Hz. A ratio of 1:1 is experimented and compared to the simulated results as shown in Figures 21 and 22. Snapshots in Figure 21 show the time corresponding to the movement of the fins, where the time duration for the servomotor to complete one cycle is 0.66 second. Therefore, it can be noticed that the time taken at the power stroke is the same as the time taken at the recovery stroke time. On the other hand,

FIGURE 19 Complete prototype robot and its environment

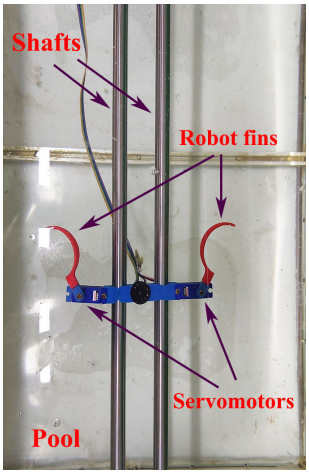

FIGURE 20 Top view of the robot in the pool

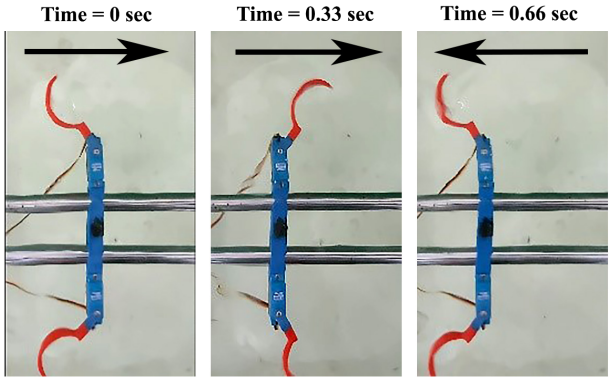

FIGURE 21 Snapshot of complete one cycle at power-to-recovery ratio of 1:1

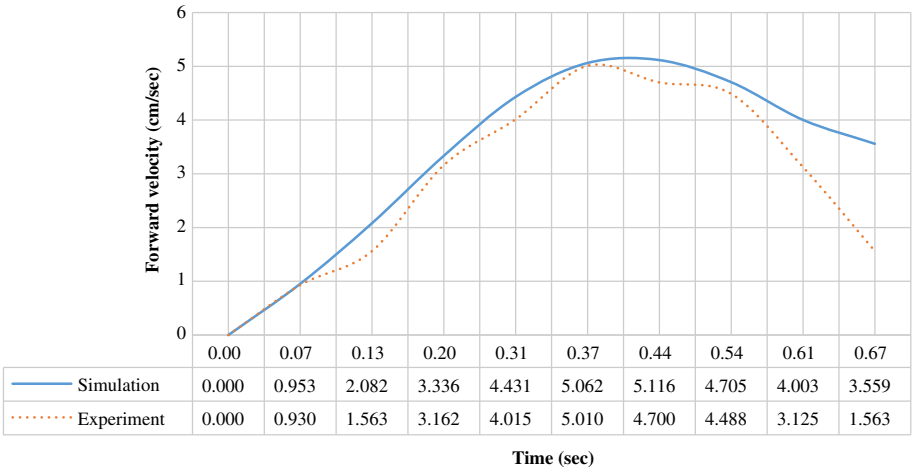

	0.00	0.07	0.13	0.20	0.31	0.37	0.44	0.54	0.61	0.67
Simulation	0.000	0.953	2.082	3.336	4.431	5.062	5.116	4.705	4.003	3.559
Experiment	0.000	0.930	1.563	3.162	4.015	5.010	4.700	4.488	3.125	1.563

FIGURE 22 Forward velocity when the power-to-stroke ratio is 1:1

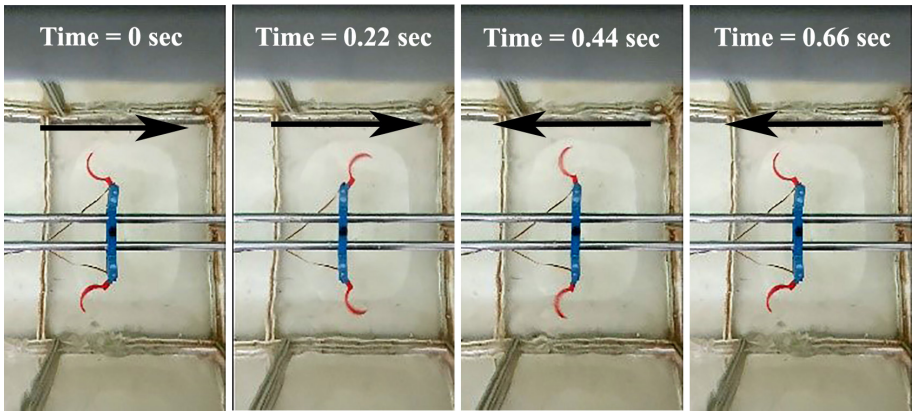

FIGURE 23 Snapshot of complete one cycle at power-to-recovery ratio of 2:1

in Figure 23, the ratio is adjusted to 2:1 where the fin will complete the power stroke at time 0.22 second, while the recovery stroke will be completed at time 0.66 second, which is twice of the time taken to complete the power stroke. In Figure 24, the power stroke will be completed at time 0.165 second, and from 0.165 to 0.66 second, the fins will complete the recovery stroke; the time taken to complete the recovery stroke is three times the time taken to complete the power stroke. In Figure 25, the velocity of the power stroke is further increased and will be completed at time 0.132 second, while the remaining time will be taken by the recovery stroke to be completed at time 0.66 second. Finally, in Figure 26, the velocity of power stroke is now five times the velocity of the recovery stroke, the power stroke will be completed at time 0.11 second, and time from 0.11 to 0.66 second will be for the recovery stroke.

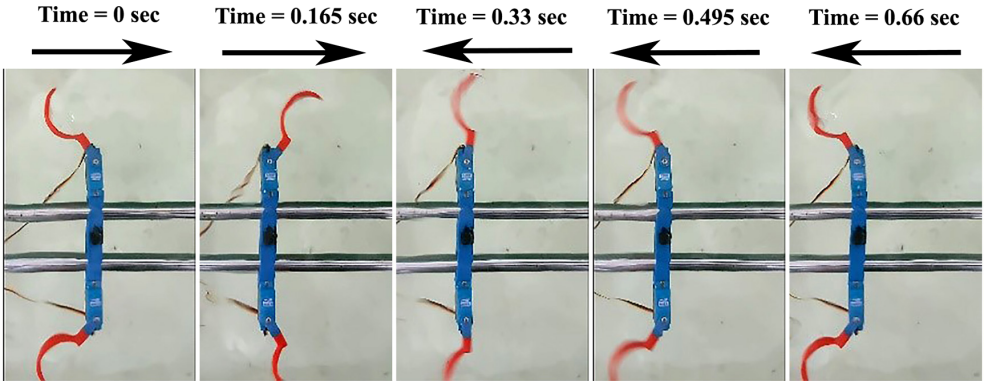

FIGURE 24 Snapshot of complete one cycle at power-to-recovery ratio of 3:1

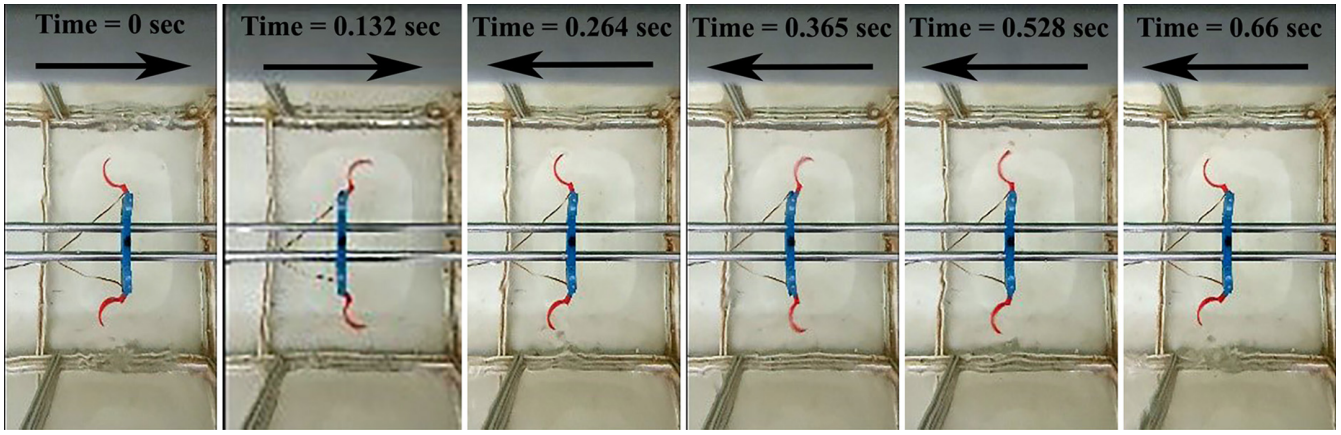

FIGURE 25 Snapshot of complete one cycle at power-to-recovery ratio of 4:1

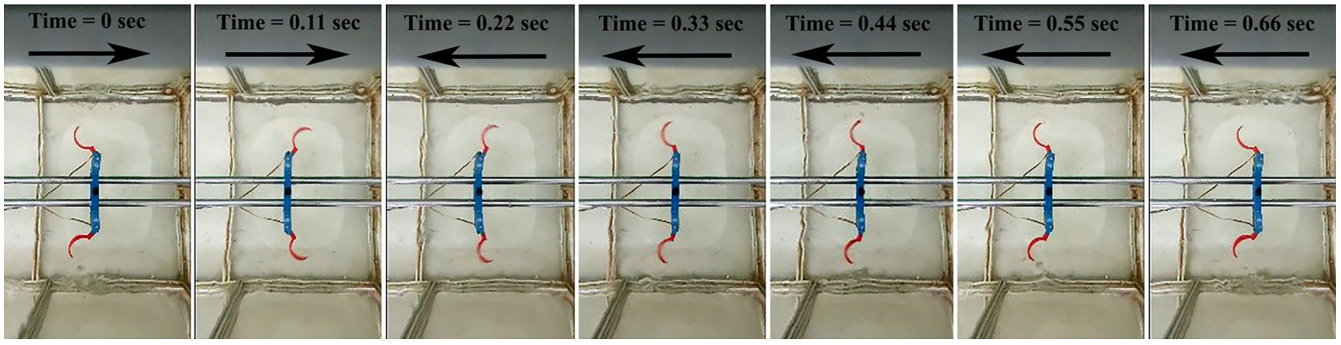

FIGURE 26 Snapshot of complete one cycle at power-to-recovery ratio of 5:1

For all the designed rigid fins, we can notice that a higher power-to-recovery ratio provides a faster swimming velocity, which matches the results shown in Figure 18. Since the drag force will be increased at high power-to-recovery ratios within the servomotor constraints, it can be noticed that the highest achievable swimming velocity does not happen at the highest power-to-recovery ratio. Instead, the highest swimming velocity is obtained if a moderate ratio (3:1) is used. When the ratio is 3:1, the drag force at the recovery stroke will no longer affect the forward velocity of the body. Figures 22 and 27-30 demonstrate this fact.

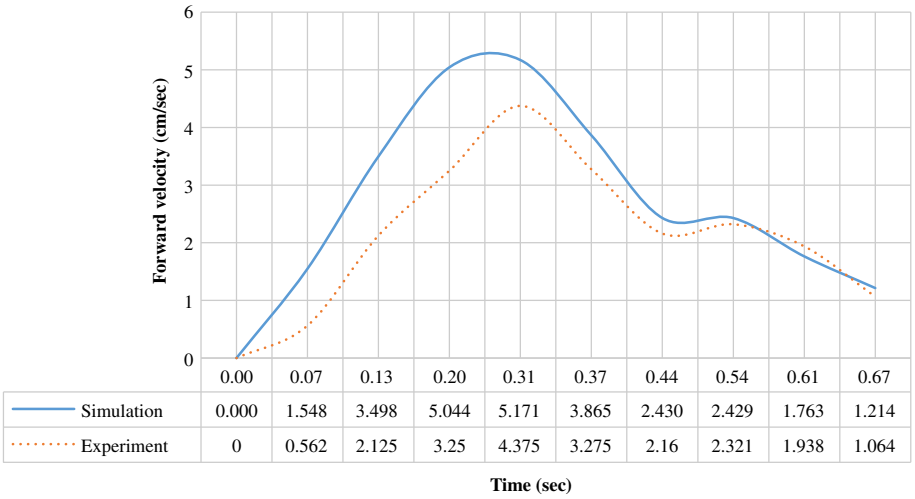

	0.00	0.07	0.13	0.20	0.31	0.37	0.44	0.54	0.61	0.67
Simulation	0.000	1.548	3.498	5.044	5.171	3.865	2.430	2.429	1.763	1.214
Experiment	0	0.562	2.125	3.25	4.375	3.275	2.16	2.321	1.938	1.064

FIGURE 27 Forward velocity when the power-to-stroke ratio is 2:1

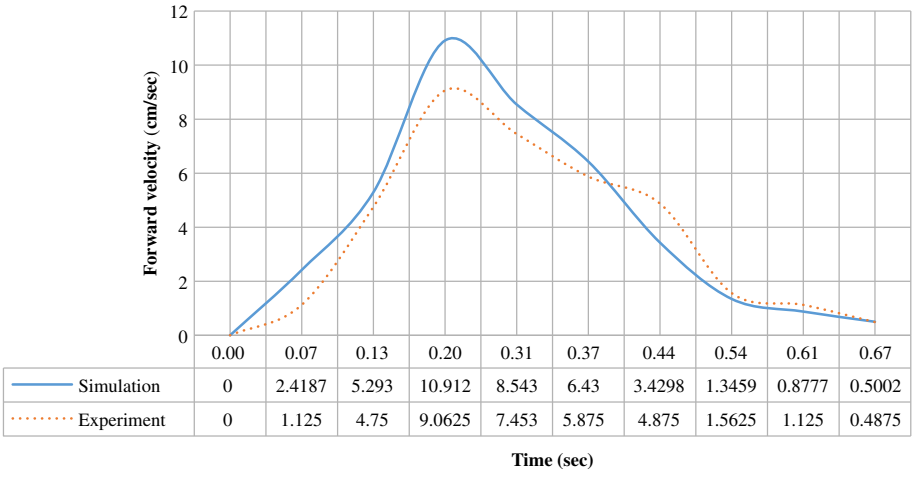

	0.00	0.07	0.13	0.20	0.31	0.37	0.44	0.54	0.61	0.67
Simulation	0	2.4187	5.293	10.912	8.543	6.43	3.4298	1.3459	0.8777	0.5002
Experiment	0	1.125	4.75	9.0625	7.453	5.875	4.875	1.5625	1.125	0.4875

FIGURE 28 Forward velocity when the power-to-stroke ratio is 3:1

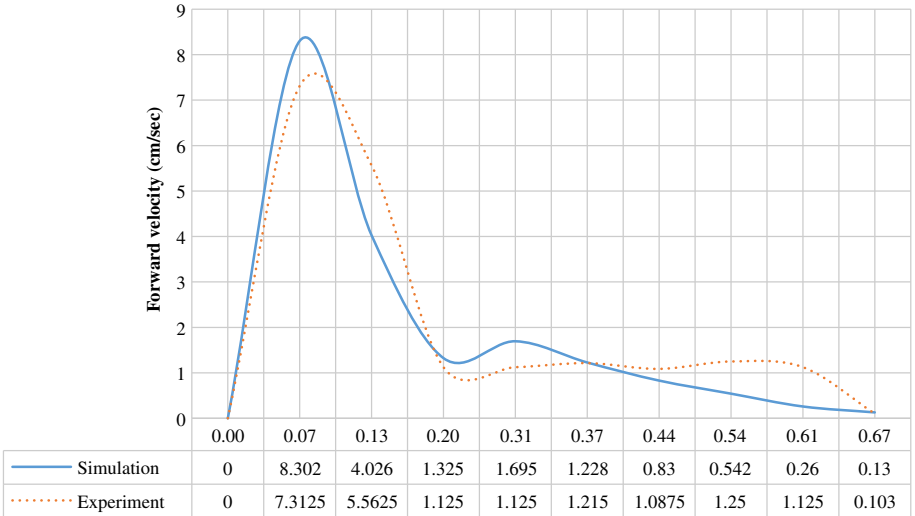

	0.00	0.07	0.13	0.20	0.31	0.37	0.44	0.54	0.61	0.67
Simulation	0	8.302	4.026	1.325	1.695	1.228	0.83	0.542	0.26	0.13
Experiment	0	7.3125	5.5625	1.125	1.125	1.215	1.0875	1.25	1.125	0.103

FIGURE 29 Forward velocity when the power-to-stroke ratio is 4:1

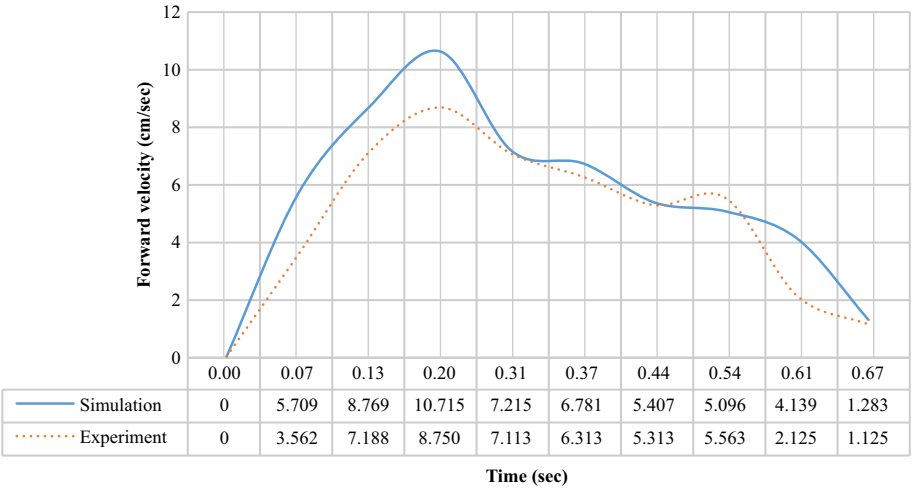

	0.00	0.07	0.13	0.20	0.31	0.37	0.44	0.54	0.61	0.67
Simulation	0	5.709	8.769	10.715	7.215	6.781	5.407	5.096	4.139	1.283
Experiment	0	3.562	7.188	8.750	7.113	6.313	5.313	5.563	2.125	1.125

FIGURE 30 Forward velocity when the power-to-stroke ratio is 5:1

5 | CONCLUSION

In this study, a novel model of the pectoral fins has been proposed as the main locomotor for labriform robotic fish. The proposed design was implemented under SolidWorks software with the aid of the CFD method. Utilizing the shape of concave fins, the hydrodynamic forces generated at the power stroke outcomes the one generated at the recovery stroke. This fact gives the robot the ability to move forward at larger displacement compared with the recovery stroke. Several fin-oscillating angles were investigated, and an optimum oscillation range was investigated for each power-to-recovery ratio. The main objective that has been achieved is a maximum thrust during the power stroke and a minimum drag during the recovery stroke. Five values of power-to-recovery ratio have been tested, the generated hydrodynamic thrust and drag are calculated, and the maximum thrust was obtained in the moderate ratio of power-to-recovery stroke of 3:1. The dynamic model was validated through experiments conducted on a robotic fish, where the swimming velocity of the robot was measured. The drag force will be increasing at the higher ratios, and it can be noticed that the highest achievable swimming velocity does not happen at the highest power-to-recovery ratio. Instead, the highest swimming velocity is obtained if a moderate ratio (3:1) is used, in which the drag force at recovery stroke will no longer affect the forward velocity of the body since it will be kept at a minimum. The results of the experiments proved the success of the proposed design, and it can be used for labriform-mode swimming robots.

CONFLICT OF INTEREST

The authors have no conflict of interest relevant to this article.

AUTHOR CONTRIBUTIONS

Farah A. Naser and Mofeed T. Rashid contributed equally to conceptualization, data curation, formal analysis, investigation, methodology, resources, software, validation, visualization, and writing-original draft; Mofeed T. Rashid contributed equally to supervision and writing-review and editing.

ORCID

Mofeed T. Rashid https://orcid.org/0000-0001-6786-8486

REFERENCES

1. Masoomi S, Chen X, Gutschmidt S, Sellier M. Efficiency-based optimization of a 2-DOF robotic fish model. *Int. J. Biomechatron Biomed Robotics*. 2013;2(2/3/4):93-101.
2. Sitorus PE, Nazaruddin Y, Leksono E, Budiyono A. Design and implementation of paired pectoral fins locomotion of labriform fish applied to a fish robot. *J Bion Eng*. 2009;6:37-45.
3. Raj A, Thakur A. Fish-inspired robots: design, sensing, actuation, and autonomy—a review of research. *Bioinspir Biomim*. 2016;11:1-30.
4. Rashid MT, Frasca M, Ali AA, Ali RS, Fortuna L, Xibilia MG. Artemia swarm dynamics and path tracking. *Nonlinear Dyn*. 2011;68(4):555-563.

5. Rashid MT, Frasca M, Ali AA, Ali RS, Fortuna L, Xibilia MG. Nonlinear model identification for Artemia population motion. *Nonlinear Dyn*. 2012;69(4):2237-2243.
6. Rashid MT, Ali AA, Ali RS, Fortuna L, Frasca M, Xibilia MG. Wireless underwater mobile robot system based on ZigBee. Paper presented at: International Conference on Future Communication Networks, Baghdad, Iraq; 2012; 117-122.
7. Cao Y, Bi S, Cai Y, Wang Y. Applying central pattern generators to control the robofish with oscillating pectoral fins. *Ind Robot*. 2015;42(5):392-405.
8. Ma H, Cai Y, Wang Y, Bi S, Gong Z. A biomimetic cownose ray robot fish with oscillating and chordwise twisting flexible pectoral fins. *Ind Robot*. 2015;42(3):214-221.
9. Behbahani SB, Tan X. Role of pectoral fin flexibility in robotic fish performance. *J Nonlinear Sci*. 2017;27(4):1155-1181.
10. Zhang S, Qian Y, Liao P, Qin F, Yang J. Design and control of an agile robotic fish. *IEEE/ASME Trans Mech*. 2016;21(4):1846-1857.
11. Li Z, Ge L, Xu W, Du Y. Turning characteristics of biomimetic robotic fish driven by two degrees of freedom of pectoral fins and flexible body/caudal fin. *Int J Adv Robot Syst*. 2018:1-12.
12. Chen Z, Hou P, Ye Z. Robotic fish propelled by a servo motor and ionic polymer-metal composite hybrid tail. *J Dyn Syst Meas Control*. 2019;141(7):071001.
13. Clark AJ, Tan X, Kmckinley P. Evolutionary multi objective design of a flexible caudal fin for robotic fish. *Bioinspir Biomim*. 2015;10:1-17.
14. Toncu G, Stanciu V, Toncu D. A simplified model for evaluation of an underwater vehicle drag. Paper presented at: Proceedings of the 2nd International Conference on Maritime and Naval Science and Engineering, Transilvania University of Brasov, Romania; 2016; 55-58.
15. Wu XA. *Rapid Development Process for Marine Propellers Through Design, Simulation and Prototyping*. St. John's, Canada: Memorial University of Newfoundland; 2010:244.
16. Bi S, Ma H, Cai Y, Niu C, Wang Y. Dynamic modeling of a flexible oscillating pectoral fin for robotic fish. *Ind Robot*. 2014;41(5):421-428.
17. Suebsaiprom P, Lin C. Maneuverability modeling and trajectory tracking for fish robot. *Control Eng Pract*. 2015;45:22-36.
18. Behbahani S, Wang J, Tan X. A dynamic model for robotic fish with flexible pectoral fins. Paper presented at: IEEE/ASME International Conference on Advanced Intelligent Mechatronics (AIM); July 9-12, 2013; Wollongong, Australia.
19. Chen Z. A review on robotic fish enabled by ionic polymer-metal composite artificial muscles. *Chen Robot Biomim*. 2017;4(24):1-13.
20. Zhong Y, Li Z, Du R. Robot fish with two-DOF pectoral fins and a wire driven caudal fin. *Adv Robotics*. 2018;32(1):25-36.
21. S K, Zhu Q. Numerical simulation of a pectoral fin during labriform swimming. *J Exp Biol*. 2010;213:2038-2047.
22. Li N, Su Y. Fluid dynamics of biomimetic pectoral fin propulsion using immersed boundary method. *Appl Bionics Biomech*. 2016;2016:1-23.
23. Hove JR, O'bryan M, Gordon S, Webb W, Weihs D. Boxfishes (Teleostei: Ostraciidae) as a model system for fishes swimming with many fins: kinematics. *J Exp Biol*. 2001;204:1459-1471.
24. Barbera G, Pi L, Deng X. Attitude control for a pectoral fin actuated bio-inspired robotic fish. Paper presented at: IEEE International Conference on Robotics and Automation, Montreal, Canada; 2011.
25. Liu H, Curet O. Swimming performance of a bio-inspired robotic vessel with undulating fin propulsion. *Bioinspir Biomim*. 2018;13(5):056006.
26. Wang W, Dai X, Li L, et al. Three-dimensional modeling of a fin-actuated robotic fish with multimodal swimming. *IEEE/ASME Trans Mech*. 2018;23(4):1641-1652.
27. Aiello BR, Hardy AR, Cherian C, et al. The relationship between pectoral fin ray stiffness and swimming behavior in Labridae: insights into design, performance and ecology. *J Exp Biol*. 2018;221:1-10.
28. Behbahani SB, Tan X. Design and modeling of flexible passive rowing joint for robotic fish pectoral fins. *IEEE Trans Robot*. 2016;32:1119-1132.
29. Wang W, Li Y, Zhang X, Wang C, Chen S, Xie G. Speed evaluation of a freely swimming robotic fish with an artificial lateral line. Paper presented at: IEEE International Conference on Robotics and Automation (ICRA); May 16-21, 2016; Stockholm, Sweden.
30. Arafatt HN, Stilwell DJ, Neu WL. Development of a dynamic model of a small high-speed autonomous underwater vehicle. Paper presented at: IEEE Conference—Oceans, Boston, MA; 2006.
31. Aureli M, Kopman V, Porfiri M. Free-locomotion of underwater vehicles actuated by ionic polymer metal composites. *IEEE/ASME Trans Mech*. 2010;15(4):603-614.
32. Pham VA, Nguyen TT, Lee BR, Vo TQ. Dynamic analysis of a robotic fish propelled by flexible folding pectoral fins. *Robotica*. 2019;35:1-20.
33. Rashid MT, Rashid AT. Design and implementation of swimming robot based on labriform model. Paper presented at: IEEE-Xplore: Al-Sadeq International Conference on Multidisciplinary in It and Communication Science and Applications (AIC-MITCSA); May 9-10, 2016; Iraq.
34. Williams T. A model of rowing propulsion and the ontogeny of locomotion in artemia larvae. *Biol Bull*. 1994;187:164-173.
35. Hoerner S. *Fluid-dynamic drag: practical information on aerodynamic drag and hydrodynamic resistance*. Backersfield, CA: Hoerner Fluid Dynamics; 1965.

How to cite this article: Naser FA, Rashid MT. Design, modeling, and experimental validation of a concave-shape pectoral fin of labriform-mode swimming robot. *Engineering Reports*. 2019;1:e12082. https://doi.org/10.1002/eng2.12082